Biochimica et Biophysica Acta 1838 (2014) 802–813

Contents lists available at ScienceDirect

Biochimica et Biophysica Acta

journal homepage: www.elsevier.com/locate/bbamem

Temperature dependence of diffusion in model and live cell membranes characterized by imaging fluorescence correlation spectroscopy

Nirmalya Bag [b,c], Darilyn Hui Xin Yap [b,c], Thorsten Wohland [a,b,c,*]

[a] Department of Biological Sciences, National University of Singapore, Singapore
[b] Department of Chemistry, National University of Singapore, Singapore
[c] NUS Centre for Bio-Imaging Sciences, National University of Singapore, Singapore

ARTICLE INFO

Article history:
Received 14 June 2013
Received in revised form 8 October 2013
Accepted 10 October 2013
Available online 25 October 2013

Keywords:
Membrane organization
Lipid phase
Activation energy
Camera-based FCS
FCS diffusion law

ABSTRACT

The organization of the plasma membrane is regulated by the dynamic equilibrium between the liquid ordered (L_o) and liquid disordered (L_d) phases. The abundance of the L_o phase is assumed to be a consequence of the interaction between cholesterol and the other lipids, which are otherwise in either the L_d or gel (S_o) phase. The characteristic lipid packing in these phases results in significant differences in their respective lateral dynamics. In this study, imaging total internal reflection fluorescence correlation spectroscopy (ITIR-FCS) is applied to monitor the diffusion within supported lipid bilayers (SLBs) as functions of temperature and composition. We show that the temperature dependence of membrane lateral diffusion, which is parameterized by the Arrhenius activation energy (E_{Arr}), can resolve the sub-resolution phase behavior of lipid mixtures. The FCS diffusion law, a novel membrane heterogeneity ruler implemented in ITIR-FCS, is applied to show that the domains in the S_o–L_d phase are static and large while they are small and dynamic in the L_o–L_d phase. Diffusion measurements and the subsequent FCS diffusion law analyses at different temperatures show that the modulation in membrane dynamics at high temperature (313 K) is a cumulative effect of domain melting and rigidity relaxation. Finally, we extend these studies to the plasma membranes of commonly used neuroblastoma, HeLa and fibroblast cells. The temperature dependence of membrane dynamics for neuroblastoma cells is significantly different from that of HeLa or fibroblast cells as the different cell types exhibit a high level of compositional heterogeneity.

1. Introduction

The plasma membrane is a semipermeable boundary which separates the interior and exterior of the cell. The basic building block of the plasma membrane is a lipid bilayer where a number of other biomolecules including different proteins, and carbohydrates are embedded in an organized manner. A widely accepted model for membrane organization is the 'lipid raft' hypothesis which states that the plasma membrane is an inhomogeneous fluid where small nano-sized (20–100 nm) domains, the so-called rafts that are enriched in cholesterol and sphingolipids, are phase segregated from the surrounding phospholipid dominated fluid matrix [1–5]. These two phases are the liquid ordered phase (L_o) and the liquid disordered phase (L_d), respectively [6,7]. Certain kinds of membrane proteins, for example glycosylphosphatidylinositol (GPI) anchored proteins, are known to partition preferentially into rafts [5,8]. Lipid rafts are crucial to regulating important cellular processes including signal transduction, membrane trafficking, and pathogen entry [9–17].

The vast diversity of the lipids in the plasma membrane can be broadly categorized into three classes: low melting unsaturated acyl chain lipids, high melting saturated acyl chain lipids and cholesterol. The melting temperature (T_m) is defined as the temperature at which the hexagonal closed packed solid ordered or gel phase (S_o) transforms into a random array of liquid disordered or fluid phase (L_d) through *trans-gauche* isomerization of the acyl chain [18]. A ripple phase (P_{β}) can also exist for some lipids at much lower temperature than T_m [19]. The S_o phase is very compact, ordered and almost immobile while the L_d phase is less rigid, disordered and mobile. The L_o phase does not exist in the thermodynamic phase diagram of single component lipids. However, it is induced when cholesterol is mixed to either gel or fluid lipids. When cholesterol is mixed with gel lipids, it 'fluidizes' the system by disrupting the long-range (global) order. On the other hand, it 'condenses' the fluid lipids by inducing short-range (local) order [20]. This new phase which has intermediate order and fluidity is called the L_o phase. The formation of the L_o phase depends on temperature and on the molar ratio of the lipid/cholesterol mixture.

Abbreviations: FCS, fluorescence correlation spectroscopy; ITIR-FCS, imaging total internal reflection-fluorescence correlation spectroscopy; ACF, autocorrelation function; PSF, point spread function; SLB, supported lipid bilayer; F, fluid lipid bilayer; FC, fluid lipid:cholesterol bilayer; FG, fluid lipid:gel lipid bilayer; FGC, fluid lipid:gel lipid:cholesterol bilayer

* Corresponding author at: Departments of Biological Sciences and Chemistry, and NUS Centre for Bio-Imaging Sciences, Blk S1A, Level 2, Lee Wee Kheng Building, National University of Singapore, 14 Science Drive 4, Singapore 117557, Singapore. Tel.: +65 6516 1248; fax: +65 6776 7882.
E-mail address: twohland@nus.edu.sg (T. Wohland).

0005-2736/$ – see front matter © 2013 Elsevier B.V. All rights reserved.
http://dx.doi.org/10.1016/j.bbamem.2013.10.009

The above-mentioned three phases have distinct diffusion behavior, which stems from their differences in physical properties. The lateral mobility is essential to control membrane structure and function. The coexistence of the phases gives rise to intriguing diffusion features that depend on a range of physical properties including area per lipid, lipid expansivity, domain size and dynamics, and line tension. Thus diffusion measurements are good means to probe plasma membrane heterogeneity. The universal Stokes–Einstein model for 3D diffusion cannot be extrapolated to 2D systems to describe membrane diffusion (Stokes' Paradox) [21]. The best approximation was proposed by Saffman and Delbrück who considered the viscosity surrounding the lipid sheet as one of the mediators of the diffusion and treated the problem with 3D continuum hydrodynamic theory [22]. Recent studies have shown that the Saffman–Delbrück model is valid for proteins with a hydrodynamic radius of $\leq$8 nm [23–25]. For proteins with a hydrodynamic radius of more than 10 nm a Stokes–Einstein-like model, as proposed by Gambin et al. [26], describes the data better [27]. Although these models can describe the diffusion of proteins in the membrane, they fail to explain lipid diffusion since the latter is significantly affected by the inherent viscosity of the membrane, diffusants' size, and the tilt angle with respect to the bilayer normal. A more convenient model for lipid diffusion is the semi-quantitative 'free area model' [28]. This model is a direct extrapolation of the 3D free volume model for diffusion in a gas. According to this model, diffusion occurs in the following three steps. First, a transient void is created in the lipid matrix by thermal density fluctuations. Second, one of the surrounding lipids hops into the void which has to be larger than a certain critical size. The third step is the repletion of the void created by the second lipid by other surrounding lipids. Note that this model represents diffusion as a function of free area (void) instead of viscosity. Since the model is derived from the kinetic theory of gases, it has a weak dependence on temperature and no activation energy is implied in lipid hopping. However, lipid hopping must be an activated process due to the van der Waals' interactions with the surrounding lipids. Thus a more generalized approach, the so-called Macedo–Litovitz hybrid model, was proposed by including an activation energy (E_A) term [29,30]. E_A accounts for the energy barrier the lipids have to overcome for hopping to their new locations assuming both the states before and after hopping are in equilibrium. It also incorporates the viscous drag due to the opposite monolayers, the effect of the surrounding fluid or surface, and the energy required to create a void. Since both the hopping frequency and the density fluctuations are temperature dependent, diffusion is a thermally activated process. Thermally activated processes in reaction kinetics with the initial and final states at equilibrium are described by the Arrhenius equation. The effective activation energy (E_{Arr}) term in the Arrhenius equation is interpreted in a very similar fashion to that of E_A in the free area model. Computation of E_A from E_{Arr} has been done with the knowledge of free area and the cross-sectional area of the lipid under question, which shows that the temperature dependence of lateral diffusion in membranes can be successfully explained by the free area theory [31,32]. The degree of lipid packing (van der Waals' interactions), which is one of the major determinants of the membrane phase, is directly related to the availability of free area for diffusion. Thus the temperature dependence of diffusion can provide direct evidence of the membrane phase behavior.

Fluorescence correlation spectroscopy (FCS) is a widely used technique to study membrane dynamics at the single molecule level [33–35]. Here we used camera-based imaging total internal reflection fluorescence correlation spectroscopy (ITIR-FCS) to measure membrane diffusion [36]. ITIR-FCS possesses a number of important advantages over conventional single spot FCS. This calibration-free technique allows parallel measurements of diffusion coefficients at every diffraction limited spot over a large membrane area (in this study, $5 \times 5\ \mu m^2$) [37,38]. Moreover, TIR illumination significantly reduces background arising from the bulk since only molecules close to the surface are excited. In this article, we show the temperature dependence of diffusion in one, two and three component glass-supported lipid bilayer (SLB) model systems and the corresponding E_{Arr} values are calculated from the Arrhenius equation. We show that each phase has a characteristic E_{Arr} value. A phase change is directly indicated by a change in the magnitude of E_{Arr}. We also show that the spontaneous phase reorganization upon external perturbations, e.g. cholesterol extraction, can be detected from the change of E_{Arr}. FCS diffusion law analysis [38,39] is performed to observe the sub-resolution detail of membrane diffusion which is effectively mediated by lateral membrane organization. It shows that the size and dynamics of the domains are quite different for S_o–L_d and L_o–L_d phases. Finally, we extend our study to the plasma membrane of three commonly used live cells; namely HeLa, neuroblastoma (SH-SY5Y), and fibroblast (WI-38) cells.

2. Materials and methods

2.1. Lipids and dyes

The lipids used are 1,2-dioleoyl-sn-glycero-3-phophocholine (DOPC), 1,2-dilauroyl-sn-glycero-3-phosphocholine (DLPC), 1,2-dimyristoyl-sn-glycero-3-phosphocholine (DMPC), 1,2-dipalmitoyl-sn-glycero-3-phosphocholine (DPPC) and cholesterol (Chol). Head group labeled rhodamine dye 1,2-dimyristoyl-sn-glycero-3-phosphoethanolamine-N-(lissamine rhodamine B sulfonyl) (ammonium salt) (RhoPE) was used as the fluorophore. All lipids and dyes were purchased from Avanti Polar Lipids (Alabaster, AL). Lipid and dye stock solutions were prepared in chloroform. Methyl-β-cyclodextrin (mβCD) was purchased from Sigma-Aldrich (Singapore). The stock solution of mβCD was prepared in buffer containing 10 mM HEPES and 150 mM NaCl (pH 7.4). DiI-C_{18} (1,1′-dioctadecyl-3,3,3′,3′-tetramethylindocarbocyanine perchlorate, C_{18}) was bought from Invitrogen (Singapore). The stock DiI solution was prepared in dimethyl sulfoxide (DMSO) and the concentration of the stock was calculated from the absorbance measurement in UV–Visible spectrometer (NanoDrop, Thermo Scientific, Singapore) assuming the molar extinction coefficient (ε) equals to 144,000.

2.2. Preparation of supported lipid bilayer (SLB)

Supported lipid bilayers (SLBs) were prepared by the vesicle fusion method [38,40]. In brief, calculated amounts of lipid(s) and RhoPE dye solutions were first mixed in a cleaned round bottomed flask and left in the rotary evaporator (Rotavap R-210, Buchi, Switzerland) to evaporate the solvent for at least 3 h. The thin lipid film left behind was then resuspended in 2 mL buffer containing 10 mM HEPES and 150 mM NaCl (pH 7.4). The milky lipid suspension was sonicated in a bath sonicator (FB15051 Model, Fisher Scientific, Singapore) until a clear solution was obtained, thereby forming large unilamellar vesicles. The vesicle solution was then stored at 4 °C if not used immediately. Before measurements are to be taken, the vesicle solution was first sonicated for 10 min and then 200 μL of it was placed on a cleaned cover glass ($24 \times 50-1$, Fisher Brand Microscope cover glass, Fisher Scientific, Singapore) containing 200 μL of the same buffer. The deposited vesicles were incubated at 65 °C for 20 min followed by cooling at room temperature for another 20 min. Unfused vesicles were then removed by washing with 200 μL of the buffer for at least 50 times. In the case of cholesterol depletion experiments, an mβCD solution was incubated with the sample for 30 min on the microscope stage to a final concentration of 2 mM and washed 5 times with buffer.

The cover glasses were cleaned as follows. They were first sonicated in a bath sonicator (FB15051 Model, Fisher Scientific, Singapore) with 10× diluted detergent (Hellmanex III, Hellma Analytics, Singapore) for 30 min. This was followed by rigorous washing with deioninzed (DI) water (resistivity 18.2 MΩ·cm). The cover glasses were then subjected to another sonication step for 30 min with 2 M sulfuric acid followed by

extensive rinsing with DI water. Finally, they are sonicated in DI water for 30 min. The cleaned cover glasses were stored in technical ethanol.

2.3. Cell culture, DiI staining, and GPI transfection

The cell lines used are HeLa, neuroblastoma (SH-SY5Y), and fibroblast (WI-38) cells. Adherent cells were cultivated in DMEM (Dulbecco's Modified Eagle Medium; Invitrogen) medium, supplemented with 10% FBS (fetal bovine serum; Invitrogen) and 1% PS (penicillin, and streptomycin) at 37 °C in 5% (v/v) CO_2 humidified environment. For DiI staining solution, the stock DiI solution was diluted to a final concentration of 50 nM with phenol red free DMEM medium. The culture medium (DMEM, 10% FBS and 1% PS) was first removed from the cover dish (Chamber mounted on #1.0 borosilicate cover glass with cover, 8 units, Nunc) which was seeded with cells beforehand. The 50 nM DiI solution was then added into the cover dish and incubated at 37 °C for 30 min. After 30 min, the cover dish was then rinsed with phenol red free medium (DMEM and 10% FBS) twice before adding the phenol red free medium into the cover dish for imaging. GFP–GPI plasmid was a kind gift from John Dangerfield, Anovasia Pte Ltd, Singapore. GFP–GPI was transfected using Neon™ Transfection System from Invitrogen (Singapore). HeLa cells were plated and transfected in glass covered dishes (35 mm Petri dish, 14 mm Microwell, No. 1.0 cover glass (0.13–0.16 mm), MatTek Corporation, US). The transfections were performed 20–24 h before measurements. After transfection, cells were grown in the cell culture medium (DMEM and 10% FBS). Before imaging, the cells were washed twice with phenol red free medium (DMEM and 10% FBS) and measured in phenol red free medium (DMEM and 10% FBS).

2.4. Camera-based FCS data acquisition and analysis

The instrumental setup was constructed with an inverted epi-fluorescence microscope (IX-71, Olympus, Singapore) and a high NA oil immersion objective (PlanApo 100×/1.45, Olympus, Singapore). For illumination, 532 nm (Cobolt Samba, Sweden; for RhoPE and DiI measurements), and 488 nm (Spectra-Physics Lasers, Mountain View, CA, USA; for GFP–GPI measurements) lasers were used. Through a combination of two tilting angle mirrors and a single-mode fiber, a laser beam was introduced into the microscope. The incident beam was then focused by the lenses onto the back focal plane of the objective after reflection by a dichroic mirror (495LP and Z488/532RPC for 488 nm and 532 nm excitations respectively). The objective immersion medium used was mineral oil (refractive index 1.516 at 23 °C, Olympus). Using a combination of tilting mirrors, total internal reflection (TIR) was obtained. The sample signal was passed through the same objective and dichroic mirror. The signal was filtered by emission filters (495LP and Z488/532M for 488 nm and 532 nm excitations respectively) before imaging on the camera chip. A back-illuminated EMCCD (electron multiplying charge coupled device) camera (Andor iXON 860, 128 × 128 pixels, Andor Technology, US) which was mounted on the side port of the microscope was used for imaging. The image acquisition software was Andor SOLIS for imaging (version 4.18.30004.0). In general, a stack of 50,000 frames was taken from a selected ROI (region of interest) of 21 × 21 pixels with 1 ms (for RhoPE and DiI experiments) or 4 ms (for GFP–GPI experiments) acquisition time per frame ($\Delta\tau$) and 10 MHz read-out speed per pixel. The $\Delta\tau$ is the summation of integration time (exposure time) and frame transfer time of the camera. The frame transfer time of the camera for 21 × 21 pixels ROI is 0.26 ms. Thus the integration times were 0.74 ms (for RhoPE and DiI experiments) or 3.74 ms (GFP–GPI experiments). The data was stored as 16-bit *Tiff* files. Intensity values obtained for each pixel were then temporally correlated using the 'ImFCS' — an Igor Pro (Wavemetrics, Lake Oswego, OR) based home-written software [available at http://staff.science.nus.edu.sg/~chmwt/ImFCS.html] to calculate the autocorrelation functions (ACFs) from individual pixels [41]. Through the same software, ACFs were analyzed with a suitable mathematical model (Eq. (1)) to calculate the diffusion coefficient (D) and number of particles (N).

$$G(\tau)=\frac{1}{N}\left[\mathrm{erf}(\mathrm{k})+\frac{1}{\mathrm{k}\sqrt{\pi}}\left(\mathrm{e}^{-\mathrm{k}^2}-1\right)\right]^2+G_\infty;\ \mathrm{k}=\frac{a}{2\sqrt{D\tau+\sigma^2}} \tag{1}$$

where $G(\tau)$ is the ACF as a function of correlation time (τ), N is the number of particles per pixel, a is the pixel side length, D is the diffusion coefficient, σ is the standard deviation of the Gaussian approximation of the microscope point spread function (PSF), G_∞ is the convergence of $G(\tau)$ at long correlation times. A set of representative ACFs obtained from SLBs and plasma membranes and the corresponding fits are given in Supplementary materials (Fig. S1).

The imaging conditions (instrumental parameters and fluorophore physical properties, for example, brightness and photostability) used in all the experiments in this article were in accordance with the protocol presented recently [42]. The main parameters required to optimize for an imaging FCS measurement are acquisition time per frame ($\Delta\tau$), number of frames (n), and total acquisition time (T_{aq}). Note that T_{aq} is related to $\Delta\tau$ and n as: $T_{\mathrm{aq}}=\Delta\tau\times n$. These parameters should meet the following conditions for accurate and precise results. 1) Number of frames (n) should by at least 10,000 for accurate estimation of D. However, precision increases if more number of frames are collected. 2) $\Delta\tau$ must be at least 10 times smaller than the diffusion time (τ_{d}) across the observation area of the sample under study. For instance, typical τ_{d} of a DOPC SLB at 298 K is about 45 ms. Therefore, the camera should be operated with acquisition time per frame 4.5 ms or less. 3) Total acquisition time (T_{aq}) must be 100 times larger than the τ_{d}. Since T_{aq} is related to $\Delta\tau$ and n which must be at least 10,000 for accurate measurements, one should use the following condition for the optimal T_{aq}:

$$T_{aq}\geq\max(100\tau_{\mathrm{d}},10,000\Delta\tau). \tag{2}$$

The upper limit of T_{aq} is determined by the photostability of the fluorophore. Therefore, one should choose n and $\Delta\tau$ such that T_{aq} satisfies Eq. (2) and the sample does not photobleach during acquisition.

2.5. FCS diffusion law

The FCS diffusion law describes the dependence of the transition time (τ_{d}) of a particle through an observation area on the size of the area (A_{eff}) [39,43]. The observation area (A_{eff}) in ITIR-FCS is given by the convolution of the detection area (pixel area, $A=a^2$) with the PSF (i.e., $A_{\mathrm{eff}}=A\otimes\mathrm{PSF}$) and this defines the actual membrane area over which particles are observed [42]. For Brownian free diffusion the diffusion coefficient (D) is invariant over the observation area and thus τ_{d} linearly converges to 0 for $A_{\mathrm{eff}}\rightarrow 0$. However if the membrane is not homogeneous, D can vary with position (for example, hindered diffusion by domains). In this case, τ_{d} depends on A_{eff} as follows for all A_{eff} values larger than the size of the inhomogeneities (e.g. domains):

$$\tau_{\mathrm{d}}(A_{\mathrm{eff}})=\tau_0+\frac{A_{\mathrm{eff}}}{D}. \tag{3}$$

Here τ_0 is the y-intercept and takes zero and non-zero values for free and hindered diffusion, respectively. Positive and negative τ_0 values correspond to hindered diffusion due to microdomains in which the probe can partition, or to barriers of the cytoskeleton meshwork, respectively [39]. In ITIR-FCS, various observation areas are created by pixel binning post-acquisition, i.e. the grouping of single pixels into larger areas by summing their values [38,42]. For $n\times n$ binning the observation area is $A_{n,\ \mathrm{eff}}=(n\times a)^2\otimes\mathrm{PSF}$. This eliminates the requirement of multiple measurements at different sizes of observation areas, which is technically demanding.

2.6. Temperature dependence study and Arrhenius equation

For temperature dependence measurements (between 298–313 K for SLBs and 298–310 K for plasma membrane), an incubator (Live Cell Instrument, CU-109, Zeiss, Singapore) and a CO_2/Air gas chamber (Live Cell Instrument, FC-5, Zeiss, Singapore) for cell measurements, which can be fitted on the stage of the TIRF microscope, were used. In the study, measurements at four different temperatures were done and an equilibration time of 1 h was allowed between temperature changes before measurements were taken. For each temperature, 5–10 measurements (for SLBs) or 3 measurements (for cells) per sample were taken. The experiments were repeated for at least three samples and the diffusion coefficients at the different temperatures were averaged over the number of repeat experiments conducted. The temperature dependence follows the Arrhenius dependence as shown in Eq. (4). The Arrhenius plot is obtained, through the use of Eq. (5), by plotting ln(D) against $1/T$ and E_{Arr} is obtained from the slope of the graph.

$$D = D_0 e^{-\frac{E_{Arr}}{RT}} \tag{4}$$

$$\ln(D) = \ln(D_0) - \frac{E_{Arr}}{RT} \tag{5}$$

where D is the diffusion coefficient [m^2/s], D_0 is the pre-exponential factor [m^2/s], T is the absolute temperature [K], E_{Arr} is the activation energy [J/mol] and R is the molar gas constant.

3. Results and discussions

The temperature dependence of the RhoPE labeled SLBs containing single and multiple lipids, and the plasma membrane of different cells will be discussed in the following sub-sections. We refer to the SLBs as follows: single component bilayer (F), two component bilayer containing fluid lipid and cholesterol (FC), two component bilayer containing fluid and gel lipids (FG), and three component bilayer containing fluid lipid, gel lipid and cholesterol (FGC).

3.1. Temperature dependence of supported lipid bilayer (SLB) diffusion

3.1.1. Single component bilayers (F)

DLPC (T_m = 272 K) and DOPC (T_m = 253 K) remain in the L_d phase at the experimental temperature regime (298 K–313 K). The D of both bilayers labeled with RhoPE increases about 50% from 298 K to 313 K revealing a similar temperature dependence (For DLPC: D (298 K) = 2.37 ± 0.78 μm^2/s and D (313 K) = 3.51 ± 0.98 μm^2/s and for DOPC: D (298 K) = 2.46 ± 0.90 μm^2/s and D (313 K) = 3.40 ± 1.20 μm^2/s) (Figs. 1A and C, and 2A; and Table 1). The D values reported here are obtained from a large number of experimental autocorrelation functions (N_{ACF} column in Tables 1 and 2) measured over a number of independent experiments. The standard deviation (SD) of D provides the heterogeneity of the samples across different preparations. The p-value (calculated by a two-tailed unpaired t-test) obtained between two independent measurements of a given bilayer at a given temperature is >0.7 while that for two different bilayers are ≪0.00001 showing good reproducibility between same bilayer and distinguishability between different bilayers. The standard error of the mean (SEM) of D is less than 1% in all cases. The E_{Arr} values for DLPC and DOPC SLBs are quite similar ranging between 17 and 20 kJ/mol (Table 1). These values fall in the regime of the free energies of the commonly observed intermolecular interactions in biological systems. For reference, the free energy of hydrogen bonding is 12–20 kJ/mol at 310 K. The E_{Arr} values are also quite similar to those of previous reports (16–33 kJ/mol) obtained from fluorescence methods or simulation [44,45]. This regime is slightly smaller compared to the ones from NMR studies (28–40 kJ/mol) [31]. However, the ratio of E_{Arr} values of different phases obtained here is quite comparable to that of NMR studies as will be discussed in the next sections. In fluid bilayers, the lipids have to overcome only minimal van der Waals' interactions impeded

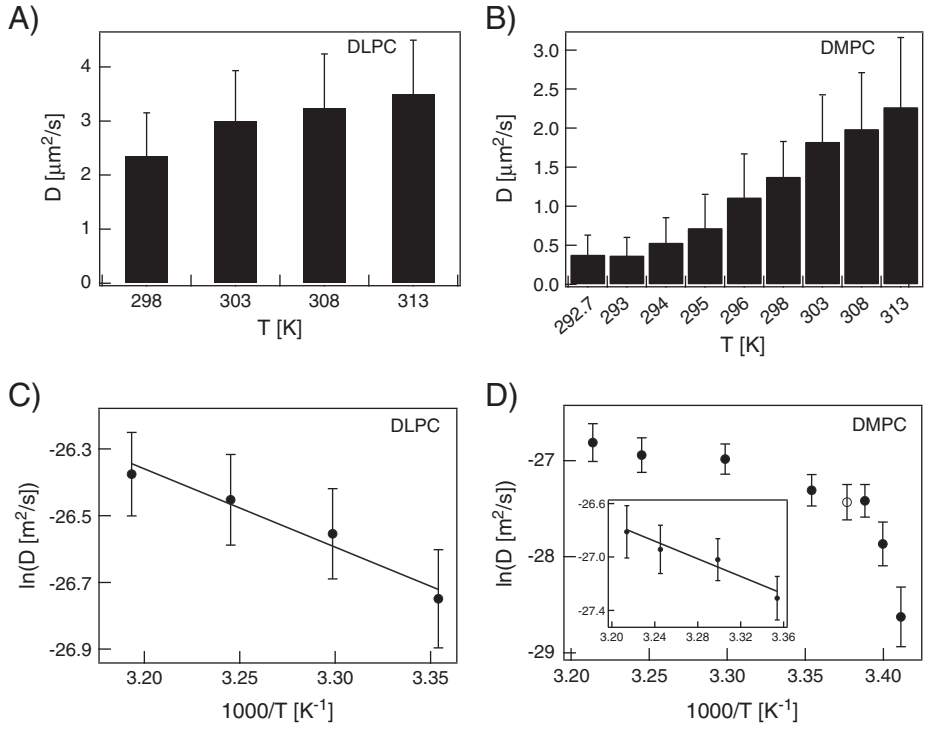

Fig. 1. Temperature dependence of diffusion coefficient and the corresponding Arrhenius plots. The temperature dependence of the diffusion of A) DLPC, and B) DMPC bilayers. The Arrhenius plots are shown in C) DLPC and D) DMPC. The open circle in D) corresponds to the transition temperature of DMPC. In the inset, the fit of the Arrhenius plot consisting of the points above the transition temperature is shown.

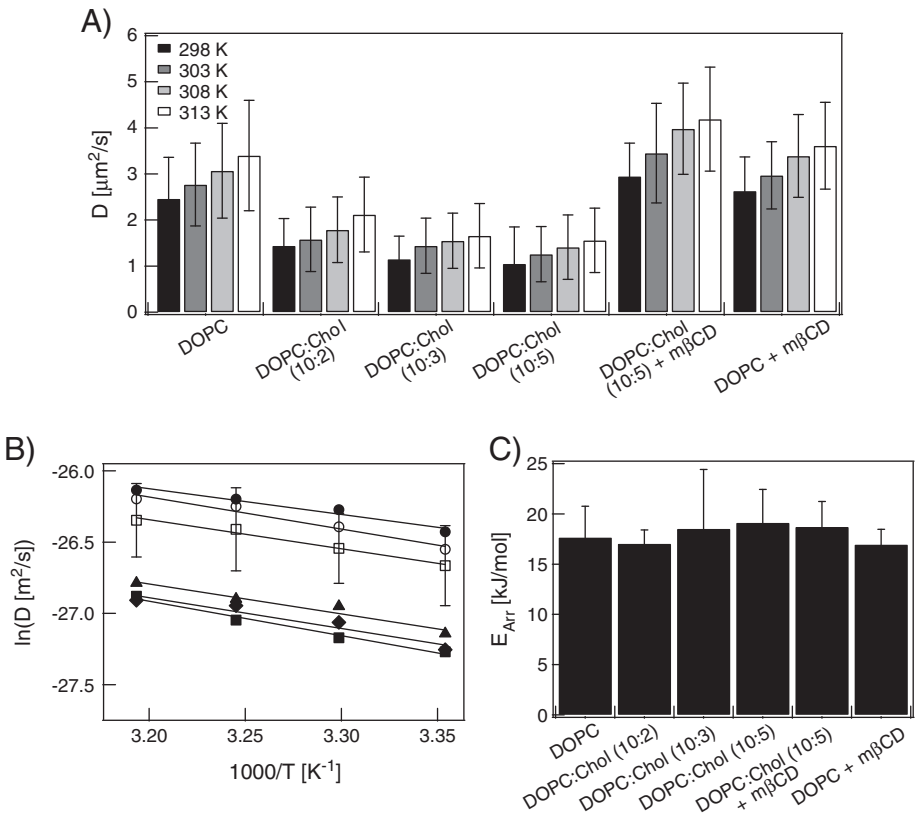

Fig. 2. Temperature dependence of bilayer lateral diffusion, corresponding Arrhenius plots and the activation energies for one (fluid lipids) and two component (containing fluid lipid and cholesterol) lipid bilayers. A) The variation of diffusion coefficients as a function of temperature. Diffusion coefficient of fluid DOPC is higher than that of fluid DMPC at a given temperature. Addition of cholesterol monotonically decreases the diffusion coefficient of DOPC bilayers. Cholesterol removal by mβCD from DOPC:Chol bilayers retrieves back the diffusion of DOPC bilayers. B) Arrhenius plots show almost similar steepness for all DOPC and DOPC:Chol bilayers. DOPC (solid circle), DOPC:Chol (10:2) (solid triangle), DOPC:Chol (10:3) (solid square), DOPC:Chol (10:5) (solid diamond), DOPC + mβCD (open square), DOPC:Chol (10:5) + mβCD (open circle). The error bars for all the data points are not shown for clarity of the figure. It is only shown for DOPC + mβCD data and the errors of all other data points are some similar percentage to their respective averages. Therefore, addition of cholesterol induces some short range order to modulate diffusion coefficient without generating a new phase. C) The E_{Arr} values are almost the same for DOPC and DOPC:Chol bilayers and do not alter on cholesterol removal from DOPC:Chol bilayers (~17–20 kJ/mol) supporting the existence of a single fluid phase in all bilayers. DMPC bilayers show higher E_{Arr} compared to DOPC bilayers.

by the loosely packed neighboring lipid matrix. Thus the diffusion of these bilayers shows only little temperature dependence.

RhoPE labeled DMPC bilayers (T_m = 296 K) shows two phases within the working temperature range (292–313 K). The data in Table 1 corresponds to temperatures above T_m. The phase transition can be clearly observed in Fig. 1B. The mobility jumped significantly once the T_m is crossed. This is more obvious in the Arrhenius plot shown in Fig. 1D. The inflection point (open circle) corresponds to the T_m. The difference in the slope directly shows the strong (right part) and weak (left part) temperature dependences for S_o and L_d phases respectively. The E_{Arr} (calculated for the temperatures above T_m) is much higher (27.10 ± 6.30 kJ/mol) than that of DLPC or DOPC (Table 1). This is because the measurement temperature range is very close to the T_m for DMPC. At this temperature regime the cross sectional area of DMPC is smaller than that of DLPC or DOPC revealing more structural compactness of the former [46]. This is evident in the diffusion coefficient of DMPC at 298 K, which is almost half compared to that of DLPC or DOPC at the same temperature. However as temperature rises, the difference in cross sectional area gradually drops and almost vanishes at 333 K [46]. The thermal area expansivity of DMPC at a given temperature within the working range is also higher than that of DLPC or DOPC [46]. For example, the thermal area expansivities of DMPC and DLPC are 0.0032 K^{-1} and 0.0028 K^{-1}, respectively, at 303 K. Since the cross sectional area of DMPC in the fluid phase increases much faster compared to that of DOPC or DLPC, a stronger temperature dependence of the former is expected. This is shown in the inset of the Fig. 1D and Table 1.

3.1.2. Two component bilayers containing fluid lipid and cholesterol (FC)

In this category, cholesterol is added to DOPC bilayers and the temperature dependence of diffusion is measured as a function of cholesterol content in the bilayer. Cholesterol is known to induce short range order in fluid bilayers which renders the bilayer more rigid. This short range ordering effect is observed in the diminution of the diffusion coefficient when cholesterol is added to an otherwise disordered DOPC fluid bilayer (Fig. 2A and Table 1). The drop in D is proportional to the cholesterol content in the bilayers, supporting membrane ordering (form 2.46 ± 0.90 μm²/s to 1.05 ± 0.40 μm²/s for 33 mol% of cholesterol at 298 K). This monotonic decrease of D agrees with NMR measurements [31] and the calculations based on the 'free area theory' [32]. However, this ordering is not sufficient to alter the membrane to a liquid ordered phase since E_{Arr} (17–20 kJ/mol) hardly changes with cholesterol (Fig. 2B and C; and Table 1).

3.1.3. Two component bilayers containing fluid and gel lipids (FG)

This group of bilayers contains both gel and fluid lipids and is RhoPE labeled. The transition temperatures of the fluid lipids (T_m (fluid) = 272 K and 253 K for DLPC and DOPC respectively) are smaller than the experimental temperatures used while the transition temperature of the gel lipid (T_m (gel) = 314 K for DPPC) is larger than the experimental temperature used. The mixed bilayers show ~2.4 times lower D compared to single component fluid ones at 298 K (Table 1). For example, when 50 mol% of DPPC (T_m = 314 K) is added to DOPC (T_m = 253 K) lipids, D changes from 2.46 ± 0.90 μm²/s to 1.02 ± 0.50 μm²/s at 298 K (Table 1).

Table 1
The temperature dependence of diffusion coefficient of the RhoPE labeled supported lipid bilayers (SLBs). $D_{T\ K}$ is the diffusion coefficient at T Kelvin. E_{Arr} is the Arrhenius activation energy barrier, and N_{ACF} is the number of autocorrelation functions analyzed to obtain mean and standard deviation of D at a given temperature.

Bilayers	$D_{298\ K}$ [μm²/s]	$D_{303\ K}$ [μm²/s]	$D_{308\ K}$ [μm²/s]	$D_{313\ K}$ [μm²/s]	E_{Arr} [kJ/mol]	Phase	N_{ACF} at a given temperature
DLPC	2.37 ± 0.78	3.02 ± 0.91	3.25 ± 0.99	3.51 ± 0.98	19.53 ± 3.33	L_d	7938
DMPC	1.38 ± 0.45	1.91 ± 0.60	1.99 ± 0.72	2.27 ± 0.89	27.10 ± 6.30	S_o at <296 K L_d at >296 K	7938
DOPC	2.46 ± 0.90	2.77 ± 0.90	3.07 ± 1.30	3.40 ± 1.20	17.66 ± 3.10	L_d	15,213
DOPC:DPPC	1.02 ± 0.50	1.88 ± 0.80	2.69 ± 0.90	3.09 ± 1.10	57.75 ± 11.70	S_o–L_d	25,797
DLPC:DPPC	0.78 ± 0.43	1.63 ± 0.59	2.05 ± 0.70	2.39 ± 0.67	55.46 ± 12.89	S_o–L_d	15,876
DOPC:Chol (10:2)	1.44 ± 0.59	1.58 ± 0.70	1.79 ± 0.71	2.12 ± 0.81	17.04 ± 1.36	L_d	15,213
DOPC:Chol (10:3)	1.15 ± 0.50	1.44 ± 0.60	1.55 ± 0.60	1.66 ± 0.70	18.53 ± 5.90	L_d	27,120
DOPC:Chol (2:1)	1.05 ± 0.40	1.26 ± 0.60	1.41 ± 0.70	1.56 ± 0.70	19.12 ± 3.30	L_d	23,814
DOPC:Chol (2:1) + mβCD	2.95 ± 0.72	3.45 ± 1.08	3.98 ± 0.99	4.19 ± 1.13	18.71 ± 2.52	L_d	21,168
DOPC + mβCD	2.63 ± 0.74	2.97 ± 0.73	3.39 ± 0.90	3.61 ± 0.94	16.96 ± 1.25	L_d	7056
DOPC:DPPC:Chol (5:5:2)	0.88 ± 0.40	1.03 ± 0.40	1.28 ± 0.50	1.50 ± 0.60	27.97 ± 2.10	L_o–L_d	38,697
DOPC:DPPC:Chol (1:1:1)	0.38 ± 0.10	0.45 ± 0.20	0.56 ± 0.20	0.69 ± 0.20	31.40 ± 3.00	L_o–L_d	19,182
DOPC:DPPC:Chol (1:1:2)	0.34 ± 0.10	0.45 ± 0.20	0.53 ± 0.20	0.64 ± 0.30	31.70 ± 2.90	L_o–L_d	9261
DOPC:DPPC:Chol (1:1:1) + mβCD	0.97 ± 0.20	1.24 ± 0.30	2.08 ± 0.50	2.86 ± 0.90	58.25 ± 8.80	S_o–L_d	7938
DOPC:DPPC (1:1) + mβCD	1.01 ± 0.40	1.21 ± 0.62	2.07 ± 0.62	2.66 ± 0.72	53.29 ± 7.45	S_o–L_d	7605

This is due to the reduced overall acyl chain mobility as expected. D obtained from a membrane spot (pixel) is the sum of characteristic diffusions of each phase weighted with the fraction of respective membrane area occupancy, the number and size of the domains, and the partition coefficient of the probe [47]. The membrane area occupied by fluid lipid is much higher than that of the gel lipid because of the tight packing of the latter in an equimolar gel–fluid bilayer. Moreover, the number and size of the domains in a given gel–fluid bilayer depends on the domain boundary strength (line tension) originating from the height mismatch between the lipids [48]. And the permeability of the probe into and out of the gel domains depends on the physicochemical interaction of the probe with the different bilayer components and the line tension arising from the height mismatch between the phases [48–50]. Therefore, the experimental D is a function of the interaction of the probe with different phases and the line tension at the phase boundary. Preferential interaction with one phase gives rise to stronger probe partitioning into that phase which in turn contributes stronger to the experimental D. Similarly, the higher the line tension, the lower the permeability and thus one expects stronger mobility retardation. D for DOPC:DPPC (1:1) is always larger than that of DLPC:DPPC (1:1) at a given temperature (Fig. 3A and Table 1). While DLPC has a saturated 12 carbon acyl chain, DOPC has a doubly unsaturated 16 carbon acyl chain. On the other hand, DPPC has a saturated 16 carbon acyl chain. This is shown in their respective bilayer thickness values at a given temperature (the reported bilayer thickness of DLPC and DPPC bilayers are 3.1 nm and 3.9 nm respectively at 323 K) [46]. This difference in chain lengths of the gel and fluid lipids results in a larger line tension for the DLPC:DPPC mixture compared to the DOPC:DPPC mixture and thus a larger retardation of the overall lateral mobility in the former mixture (Fig. 3A and Table 1). Since the D values of DOPC:DPPC and DLPC:DPPC can be directly correlated to the height mismatch (and thus line tension) at the domain boundary and RhoPE partitions into both phases, we infer that line tension plays an important role on the overall fluidity of the phase separated membrane. However, we cannot rule out the effects of differential RhoPE partitioning in DOPC:DPPC and DLPC:DPPC SLBs as a source of the observed differences. Note that no visible phase separation was observed in any of the studied gel–fluid bilayers. This is expected since the bilayers were formed on glass substrate and the chain length difference between the components are not sufficient to retain microscopic phase separation on glass [51,52]. However, both mixtures show similar temperature dependence (almost same E_{Arr}) indicating the same phase (S_o–L_d) at the sub-resolution regime (Fig. 3B and C; and Table 1). E_{Arr} for gel–fluid bilayers is much higher compared to fluid bilayers. This goes along with their respective free areas in a bilayer plane. Gel lipids reduce the free area due to their very tight packing and gel domains hinder the free diffusion in the surrounding fluid lipid region. This explains both the significant drop in D and rise in E_{Arr} of DOPC:DPPC or DLPC:DPPC bilayers compared to single component DOPC or DLPC bilayers. Notably, it takes 33 and 50 mol% of cholesterol and DPPC lipids, respectively, for an equal reduction of diffusion coefficient of DOPC at 298 K (Table 1). The mixing of cholesterol with DOPC causes a change in global order (DOPC without cholesterol is completely disordered) while sub-resolution phase segregation happens for the DOPC:DPPC mixture. This is supported also by the entirely different temperature dependence of the two systems (Figs. 2B and 3B).

3.1.4. Three component bilayers containing fluid lipid, gel lipid, and cholesterol (FGC)

This set of RhoPE labeled bilayers contains DOPC, DPPC and cholesterol. The temperature dependence of the diffusion is performed as a function of cholesterol content in a fixed molar ratio of DOPC:DPPC (1:1). The diffusion coefficient of DOPC:DPPC at 298 K does not change significantly when 17 mol% of cholesterol was added (1.02 ± 0.50 μm²/s and 0.88 ± 0.40 μm²/s respectively) (Fig. 3A and Table 1). In contrast, D drops about 40% when the same amount of cholesterol was added to the disordered DOPC bilayer at the same temperature (2.46 ± 0.90 μm²/s and 1.44 ± 0.59 μm²/s respectively) (Fig. 2A and Table 1). This reveals a stronger intermolecular interaction of DPPC/cholesterol compared to DOPC/cholesterol. Cholesterol has a flat structure with a small hydrophilic hydroxyl group at one end. DPPC having saturated, flat and rigid acyl chains shows more favorable van der Waals' interactions with cholesterol compared to that of DOPC. Since the major contribution of fluidity arises from the L_d phase, which is not populated by

Table 2
The temperature dependence of diffusion coefficient of the live cell membrane. $D_{T\ K}$ is the diffusion coefficient at T Kelvin. E_{Arr} is the Arrhenius activation energy barrier, and N_{ACF} is the number of autocorrelation functions analyzed to obtain mean and standard deviation of D at a given temperature.

Cells	$D_{298\ K}$ [μm²/s]	$D_{302\ K}$ [μm²/s]	$D_{306\ K}$ [μm²/s]	$D_{310\ K}$ [μm²/s]	E_{Arr} [kJ/mol]	N_{ACF} at a given temperature	Marker
SH-SY5Y	2.21 ± 0.71	2.32 ± 0.51	2.61 ± 0.79	2.88 ± 0.61	17.76 ± 1.61	4497	L_d (DiI)
HeLa	0.85 ± 0.23	1.07 ± 0.26	1.17 ± 0.31	1.33 ± 0.34	27.80 ± 4.58	4959	L_d (DiI)
Fibroblast	0.81 ± 0.28	0.96 ± 0.29	1.07 ± 0.26	1.30 ± 0.34	29.52 ± 4.18	6945	L_d (DiI)
HeLa	0.17 ± 0.08	0.23 ± 0.08	0.32 ± 0.11	0.38 ± 0.18	52.68 ± 3.79	7065	L_o (GPI)

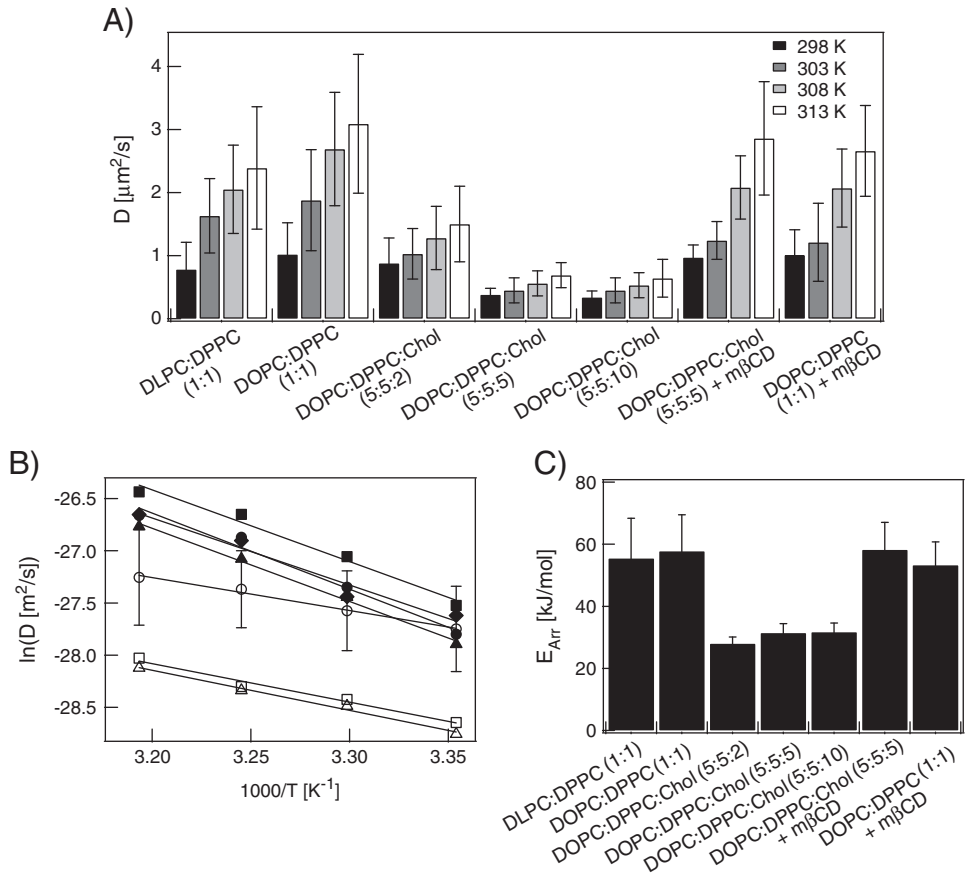

Fig. 3. Temperature dependence of bilayer lateral diffusion, corresponding Arrhenius plots and the activation energies for two (containing gel and fluid lipids) and three component (containing gel and fluid lipids and cholesterol) lipid bilayers. A) The variation of diffusion coefficients as a function of temperature. At any given temperature DOPC:DPPC bilayer shows a higher *D* than that of DLPC:DPPC bilayers revealing the stronger mixing of the latter. When cholesterol was added to DOPC:DPPC bilayers, *D* drops drastically at and above 33 mol% of cholesterol. However when mβCD (a cholesterol removing agent) was added to the DOPC:DPPC:Chol bilayer, *D* increases to the similar value of DOPC:DPPC bilayers. B) The Arrhenius plots for all the bilayers in figure A) are shown. DLPC:DPPC (solid circle), DOPC:DPPC (solid square), DOPC:DPPC:Chol (5:5:2) (open circle), DOPC:DPPC:Chol (5:5:5) (open square), DOPC:DPPC:Chol (5:5:10) (open triangle), DOPC:DPPC:Chol (5:5:5) + mβCD (solid triangle), DOPC:DPPC + mβCD (solid diamond). The error bars for all the data points are not shown for clarity of the figure. It is only shown for DOPC:DPPC:Chol (5:5:2) data and the errors of all other data points are some similar percentage to their respective averages. Bilayers containing gel and fluid lipids (DLPC:DPPC, DOPC:DPPC, and mβCD treated DOPC:DPPC:Chol) show very strong temperature dependence (steep decline in Arrhenius plot) while the three component bilayers containing cholesterol show weaker temperature dependence (gradual decline in Arrhenius plot). C) The E_{Arr} of the bilayers depicted in figure A) are shown. E_{Arr} for gel–fluid bilayers (DLPC:DPPC and DOPC:DPPC) are very high (>55 kJ/mol). On the other hand, the 'fluidizing effect' of cholesterol on gel lipids induces L_o phase in the bilayer. This, in turn, decreases E_{Arr} (~30 kJ/mol). On cholesterol depletion from the DOPC:DPPC:Chol bilayer, lipid packing spontaneously organizes to that of gel–fluid mixture as evidenced in an increase in both *D* and E_{Arr}.

cholesterol at this concentration, *D* does not alter significantly. Recently, both coarse-grained and united-atom simulations, and X-ray scattering experiments suggest cholesterol's preference for gel lipids over fluid lipids [53,54]. Interestingly, this association of cholesterol and DPPC lipids is sufficient to destroy the long range order of the latter as shown in the temperature dependence of the system. The E_{Arr} decreases dramatically as 17 mol% of cholesterol was added to DOPC:DPPC bilayers (27.97 ± 2.10 kJ/mol and 57.75 ± 11.70 kJ/mol respectively) (Fig. 3B and C; and Table 1). The disruption of long range order induces a liquid ordered phase (DPPC + Chol). Now the system has two liquid phases (DPPC + Chol and DOPC) (Fig. 6C). The boundary tension of these two phases is smaller compared to a pure DOPC:DPPC bilayers. The induction of an L_o phase by 17 mol% of cholesterol in an S_o–L_d co-existent phase has also been previously reported [55]. When the concentration of cholesterol increases, *D* decreases drastically (Fig. 3A and Table 1). *D* drops about 56% when changing cholesterol from 17 to 33 mol% (from 0.88 ± 0.40 μm²/s to 0.38 ± 0.10 μm²/s) at 298 K. This is quite similar to what was observed when 33 mol% of cholesterol was added to DOPC bilayers at 298 K. As cholesterol content increases, it starts populating the liquid disordered phase modifying its molecular composition to DOPC + Chol (Fig. 6C). However, the activation energy hardly changes since the phases are not different. Even higher cholesterol content (50 mol%) alters neither the dynamics nor its temperature dependence showing the saturation in the structural properties of the phases as expected (Fig. 3A–C, Table 1) [54,56]. The co-localization of cholesterol with different lipid species at 298 K is shown in Fig. 4. It is noteworthy that the E_{Arr} order is FG > FGC > FC ~ F. In summary, the same amount of cholesterol causes densification without any phase transition when added to DOPC bilayers (by inducing *trans* conformation in the acyl chains rendering it more ordered) and phase transition when added to DOPC:DPPC bilayers (by diminishing the line tension in the phase boundary).

3.1.5. Membrane reorganization upon cholesterol extraction

Removal of cholesterol from DOPC:Chol bilayers (FC) by mβCD restores the mobility without changing E_{Arr} (Fig. 2A–C and Table 1). The *D* of the cholesterol depleted DOPC:Chol bilayer however was slightly higher than that of the native DOPC bilayer (2.95 ± 0.72 μm²/s and 2.46 ± 0.90 μm²/s, respectively at 298 K). This might be an effect of the complex interaction of mβCD with bilayers other than just cholesterol extraction (for instance, phospholipid extraction, etc.) [57]. Nonetheless, an unaltered E_{Arr} supports the inference that all these bilayers remain in the same L_d phase regardless of cholesterol content. This observation matches with NMR results [31]. The unaltered E_{Arr} rules out

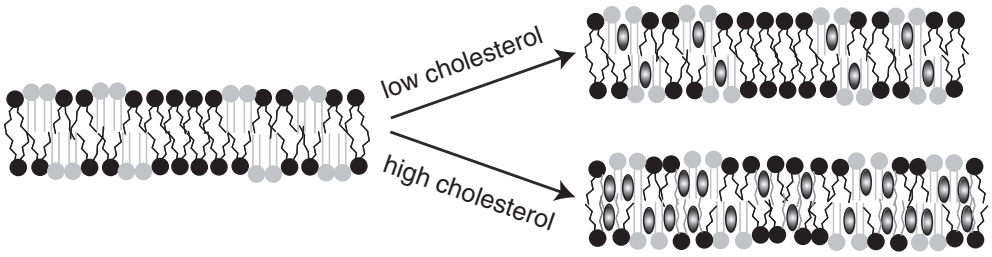

Fig. 4. Concentration dependent location of cholesterol in DOPC:DPPC:Chol bilayers at 298 K. Cholesterol preferentially co-localizes with DPPC lipids at low concentrations (17 mol%) while it is also distributed into DOPC phases at high concentration (>33 mol%). Notably, cholesterol is able to induce liquid ordered phase by disrupting the long range order in DPPC lipids even at low concentration while being partitioned preferentially in the DPPC phase.

any phase reorganization as anticipated. However when cholesterol is extracted from DOPC:DPPC:Chol bilayer (FGC), the diffusion coefficient increases with concomitant increase in activation energy (Fig. 3A–C and Table 1). Both D at a given temperature and E_{Arr} after cholesterol removal are quite similar to those of DOPC:DPPC bilayers (Table 1). This implies complete phase reorganization. We also performed mβCD treatment on DOPC and DOPC:DPPC bilayers as negative controls. They do not show any significant difference in either D at a given temperature or E_{Arr} of the respective systems. Therefore the change in E_{Arr} of FGC bilayers upon cholesterol removal is truly because of phase reorganization. It was previously reported that mβCD preferentially extracts cholesterol from the L_d phase in giant unilamellar vesicles (GUVs) [58]. However, we did not see any indication of this preference. Had cholesterol been extracted only from the L_d phase, we would not have observed the spontaneous phase change implicated by E_{Arr} and the recovery of D. This apparent ambiguity seems to originate from the size of the domains in the GUV and SLB as the authors from the earlier study also speculated [58]. The domains in GUVs are large and optically visible while those on the currently studied bilayers are smaller than the optical resolution limit. Small domains are more relevant to the biological systems and mβCD extracts cholesterol from the entire plasma membrane without any preference for the L_d phase in this case. However, the percentage of cholesterol removal depends on the concentration of mβCD and the incubation time [57,59].

3.2. Temperature dependence of live cell membrane diffusion

The temperature dependence studies were extended to live cell membranes. Three commonly used cell lines, namely HeLa, SH-SY5Y neuroblastoma, and WI-38 fibroblast cells, were investigated. DiI was used as L_d phase marker. The diffusion of SH-SY5Y membrane is much faster compared to the other two cell lines under identical experimental conditions (Fig. 5A and Table 2). For example, diffusion coefficient of DiI in SH-SY5Y is 2.88 ± 0.61 μm^2/s while those in HeLa and WI-38 are 1.33 ± 0.34 μm^2/s and 1.30 ± 0.34 μm^2/s respectively at 310 K. Moreover, the temperature dependence of DiI diffusion in SH-SY5Y cell is quite different from either HeLa or WI-38 cells (Fig. 5B and C, Table 2). The E_{Arr} values for the L_d phase are: SH-SY5Y (17.76 ± 1.61 kJ/mol), WI-38 (29.52 ± 4.18 kJ/mol), and HeLa (27.80 ± 4.58 kJ/mol). This shows that the membrane composition of the cells induces quite different dynamical behavior even within the L_d phase. Recently the heterogeneity in lateral dynamics across a range of eukaryotic cell membranes are shown by confocal FCS based diffusion time distribution analysis (DDA) [60]. It is indeed known that HeLa cells have very high protein content in the plasma membrane while WI-38 cells have large raft fractions [61]. We then measured the temperature dependence of GFP–GPI diffusion in HeLa cells. GFP–GPI is a L_o marker. Here a very strong temperature dependence (E_{Arr} = 52.68 ± 3.79 kJ/mol) is observed as anticipated. Interestingly, the ratio of E_{Arr} for L_o and L_d in HeLa cells is similar to that obtained from bilayer measurements (Tables 1 and 2).

3.3. Characterization of phase organization by FCS diffusion law

FCS diffusion law analysis describes the nanoscopic organization in membranes [39,62]. In this analysis, the diffusion time (τ_d) across membrane area is plotted as a function of the membrane area. The intercept (τ_0) of the diffusion law plot provides information about the type of membrane dynamics which correlates with the nanoscale structure. For free diffusion, τ_d scales linearly with the observation area on the membrane giving rise to a zero intercept in the FCS diffusion law plot. A positive intercept implies that the diffusion is hindered by energy barriers, e.g. membrane domains. In this case, probe molecules are transiently confined inside the domains due to dynamic partitioning across an energy barrier. FCS diffusion law analysis gives a positive intercept if the probe molecule partitions into two phases having different diffusion coefficients. Therefore, probe partitioning plays a crucial role on the outcome of FCS diffusion law analysis. For impermeable physical obstacles as present in a meshwork, the diffusant is allowed to move freely inside a mesh but it has to jump over the mesh boundary to move to the neighboring mesh. The FCS diffusion law plot gives a negative intercept in this situation.

FCS diffusion law analyses give zero intercepts (within the theoretical limit suggested in [42]) for all single component (F) and two component bilayers containing fluid lipid and cholesterol (FC) at all temperatures. This is in accordance with the temperature dependence studies which show that all these bilayers are in the L_d phase. For two component bilayers containing gel and fluid lipids (FG), a strictly positive intercept (0.245 ± 0.086 s) is observed at 298 K revealing the existence of domains while it is less positive (0.147 ± 0.067 s) at 313 K (Fig. 6A and B). This is expected since RhoPE partitions into both S_o and L_d phases which differ in fluidity. The positive intercept obtained from a S_o–L_d bilayer is in good agreement with the recent Z-scan FCS study on RhoPE labeled SLBs [63]. Note that the theoretical limit of the imaging FCS diffusion law intercept for free diffusion is ±100 ms under the current imaging condition [42]. Contrary to our results, Favard et al. obtained negative intercept for So–Ld bilayer [64]. The ambiguity between the results seems to arise from the different membrane models and fluorescent probes used in their experiments. Favard et al. used multilamellar vesicles (MLVs) labeled with either C5 Bodipy PC which is known to partition into the L_d phase, or Atto647 head labeled PE. The size and other physical properties of membrane phases and dye partitioning differ among different membranes [50,65]. The decrease of magnitude of the intercept is also reasonable since domains melt on temperature rise and the phases become more similar. The melting of domains relaxes the compactness of the S_o phase along with the usual high density fluctuations at high temperature. This combined effect leads to a strong temperature dependence of the FG bilayers as shown earlier (Fig. 3B and C; and Table 1). The existence of very small domains (<100 nm) in a DOPC:DPPC bilayer at ambient temperature was earlier observed by super-resolution imaging [66]. For three component bilayers (FGC), we observe very interesting features in FCS diffusion law analysis. At low cholesterol content (17 mol%), the intercept is slightly negative with very high standard deviation (−0.135 ± 0.102 s) at

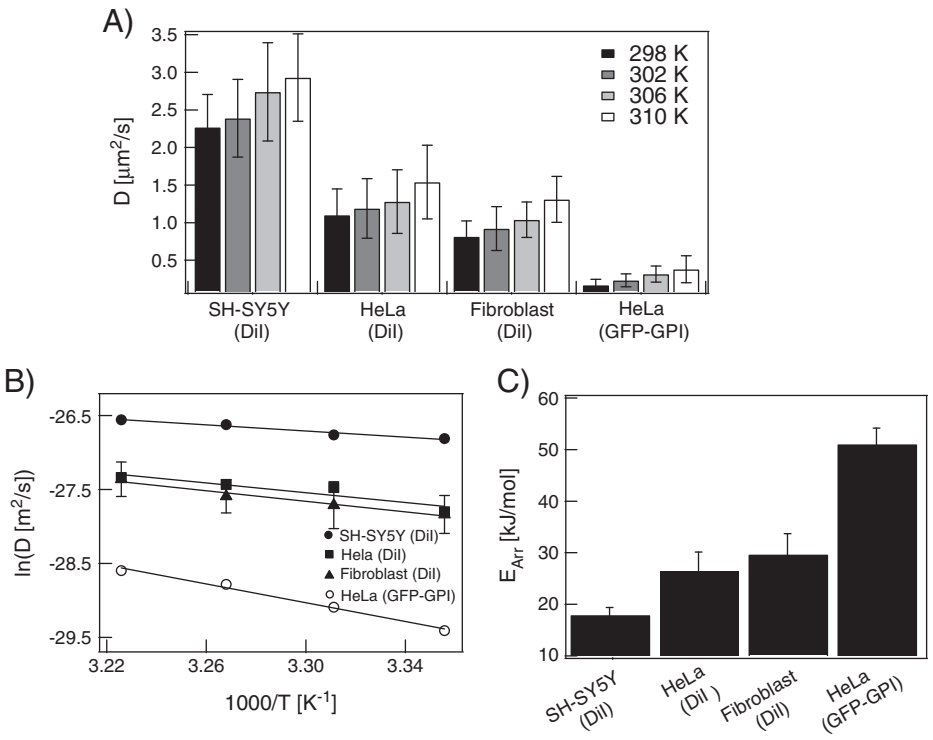

Fig. 5. Temperature dependence of lateral diffusion, corresponding Arrhenius plots and the activation energies in different live cell membranes. Both the liquid ordered phase (L_o) and liquid disordered phase (L_d) are probed by specific markers GFP–GPI and DiI-C_{18}, respectively. A) Temperature dependence shows that the fluidity of the L_d phase at a given temperature is much higher for SHSY-5Y cells compared to HeLa or fibroblast cells. The diffusion coefficient of the L_d phase is about 3.5 times higher than that of the L_o phase at physiological temperature (310 K). B) The Arrhenius plots clearly show difference in the slopes for L_d phases between SH-SY5Y and HeLa/fibroblast cells. The error bars for all the data points are not shown for clarity of the figure. It is only shown for fibroblast membrane data and the errors of all other data points are some similar percentage to their respective averages. The L_o phase, on the other hand, shows much stronger temperature dependence compared to the L_d phase as expected. C) The activation energy for lipid diffusion in the more compact L_o phase is higher than that of the L_d phase.

298 K and zero (-0.028 ± 0.036) at 313 K (Fig. 6B). Given that the *D* of DOPC:DPPC:Chol (5:5:2) and DOPC:DPPC (1:1) are almost the same at 298 K, the intercepts are quite different. This also suggests a difference in membrane phase. As the cholesterol content increases (33 mol%), we observe a strictly negative intercept (-0.492 ± 0.223 s) at 298 K which increases towards less negative values (-0.206 ± 0.118 s) at 313 K (Fig. 6A and B). The different organizational features in FG and FGC bilayers, as depicted in the sign of diffusion law intercepts, can be explained from the physical properties of the membrane. Notably we observed a negative intercept for the L_o–L_d phase co-existence. This is in contrast to the usually observed positive intercept for L_o–L_d partitioning in the case of lipid rafts in plasma membranes [39,67]. This apparent discrepancy can be addressed in the following manner. The phase separation is stabilized by the line tension at the domain boundary arising from significant height differences between the phases in FG bilayers [48]. Note that the domains in the FG bilayers studied here are smaller than the diffraction limit unlike DLPC:DSPC bilayers [38]. This is because of very high line tension domains in DLPC:DSPC bilayers arising from the large difference in the phase heights. When 17 mol% cholesterol is added to the DOPC:DPPC bilayer, the height difference decreases due to the interaction of cholesterol with DPPC (Figs. 4 and 6C). The loss in height difference decreases the line tension which makes the diffusion more free even at 298 K. Similar effects are observed in cholesterol-free DOPC:DPPC bilayers when the temperature increases as discussed earlier. At higher concentration, cholesterol becomes sufficiently abundant in the L_d phase at 298 K (Table 1). This diminishes the line tension making the phases more similar (Fig. 6C). However, the persisting height difference maintains the L_o–L_d phase coexistence. Under this scenario, one would expect the diffusion to be random and thus τ_0 to be zero. However, this intriguing deviation can be addressed by considering the fact that the decrement in line tension makes the domains shrink in size, irregular in shape, and larger in population [48,68]. These very small domains are themselves mobile and their irregular shape and high abundance could possibly form dynamic physical obstacles for the diffusion of the probe molecule unlike the static domains in the FG bilayers (Fig. 6D and E). These dynamic domains would then be responsible for the negative values as any organizational scenario that gives rise to a meshwork-like structure would have a negative intercept in the FCS diffusion law [64]. As temperature increases the diffusion becomes more normal. Overall, the FCS diffusion law analyses indicate that the line tension in the domain boundary plays a crucial role in membrane organization. The live cell membrane organization as a function of temperature is also studied by FCS diffusion law analysis. The zero intercepts obtained for DiI in HeLa cell membranes at all temperatures infer free diffusion throughout the L_d phase. For GPI as the temperature increases the intercept becomes less positive (intercept $= 3.96 \pm 0.17$ s and 1.19 ± 0.11 s respectively at 298 K and 310 K) (Fig. 7A and B). This monotonic drop is due to domain melting at high temperature as expected. The intercept for the raft partitioning of GPI is about 50–400 times higher compared to previous reports by spot variation-FCS (sv-FCS) [67] and stimulated emission depletion-FCS (STED-FCS) [69]. The difference in the absolute values is largely due to the limitation of the pixel size and the frame rate of the camera used in this study. Sankaran et al. showed that the intercept values can be reduced by reducing pixel size [42]. However, the signal to noise also decreases with pixel size, which makes FCS measurements very noisy. Therefore, the intercept value for GFP-GPI expressed cell obtained here can be taken as the calibration standard of raft dynamics studied for imaging FCS diffusion law performed by the current instrumental set-up.

In summary, we show that membrane phases can be correctly distinguished from the temperature dependence of their respective lateral dynamics. The organization of the plasma membrane is balanced by the circumstantial co-clustering of cholesterol with the available lipids in a given membrane composition. Furthermore, line tension in

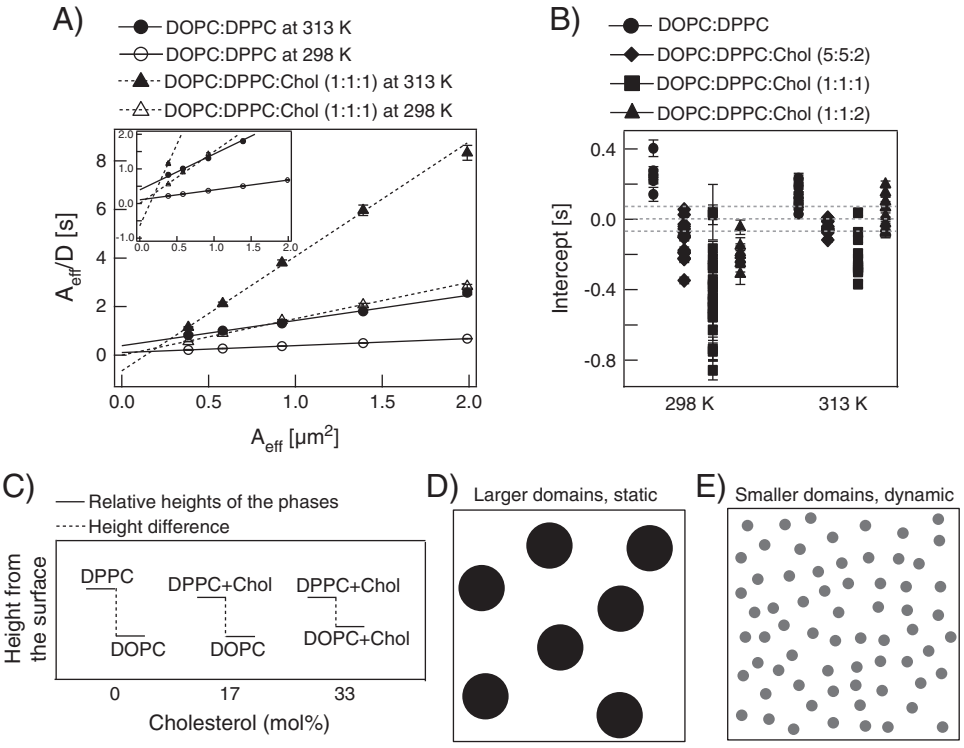

Fig. 6. FCS diffusion law analysis of the membrane dynamics of supported lipid bilayers at different temperatures. A) Representative FCS diffusion law plots for the FG and FGC bilayers at 298 K and 313 K are shown. The positive intercept of DOPC:DPPC bilayer at 298 K diminishes towards zero at 313 K. The negative intercept of DOPC:DPPC:cholesterol bilayer at 298 K also increases towards zero at 313 K. B) The distribution of intercepts for different FG and FGC bilayers are shown. C) The schematic of change in the height difference between the phases in DOPC:DPPC bilayer is shown as a function of added cholesterol concentration. The schematics of D) large and static domains in DOPC:DPPC bilayers, and E) small, dynamic domains in DOPC:DPPC:cholesterol bilayers.

the domain boundaries plays a very important role in membrane organization.

4. Conclusion

In this report, we studied the temperature dependence of diffusion of supported lipid bilayers exhibiting the three most relevant phases as well as of live cell membranes. We show that the temperature dependence of membrane dynamics which is parameterized by the Arrhenius activation energy barrier (E_{Arr}) is a useful tool to explore plasma membrane phase behavior. Compact membrane phases show stronger temperature dependence and thus have a higher E_{Arr}. The E_{Arr} for S_o–L_d and L_o–L_d phases are about 2.5 and 1.7 times higher, respectively, than that of the L_d phase. The significant differences in the E_{Arr} values across the phases thus provide a way to study membrane organization which cannot be imaged by conventional microscopy. Therefore, E_{Arr} can be used as a determinant for sub-resolution phase organization. It is also shown that cholesterol mixes with both fluid and gel lipids. However, it shows preference to gel lipids over its fluid counterpart in a mixture. Furthermore, 17 mol% cholesterol is sufficient to introduce a L_o phase in a mixed S_o–L_d phase. The novel integration of the FCS diffusion law in ITIR-FCS allows us to observe the detailed structural organization in the membrane. We show that the decrease in line tension causes the formation of small and mobile domains which eventually act as physical barriers for diffusion. On the other hand, temperature induced domain melting can be tracked by the modulation of the FCS diffusion law intercept in both model and plasma membranes. Thus the study of temperature dependence of membrane diffusion by ITIR-FCS in conjunction

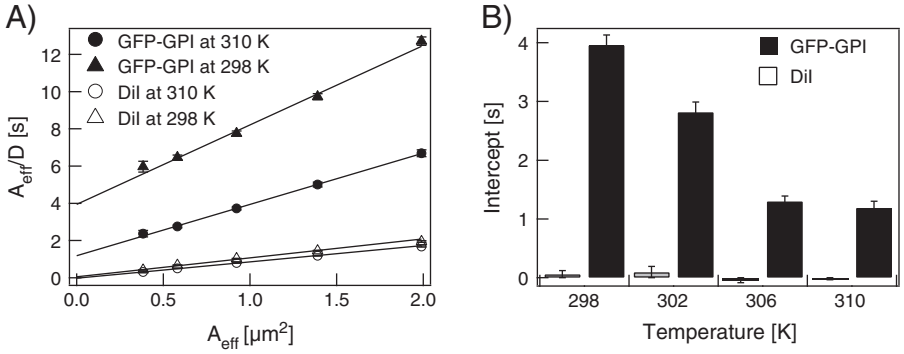

Fig. 7. FCS diffusion law analysis of the membrane dynamics of HeLa cells at different temperatures. A) Representative FCS diffusion law plots for DiI (L_d marker) and GFP–GPI (L_o marker) at 298 K and 313 K are shown. GPI always show strict positive intercepts while the intercepts for DiI are always zero. This reveals the free and hindered diffusions respectively in L_d and L_o phases. B) The temperature dependence of the FCS diffusion laws intercepts is shown. The intercept gradually decreases at the temperature increase. However, a strict positive value even at 310 K reveals the existence of a significant amount under domains at physiological conditions.

with the FCS diffusion law is an elegant method to decipher dynamic membrane organization. It will be interesting to observe the change in membrane phases via E_{Arr} and the FCS diffusion law upon external perturbations by pharmacological drug treatments, heat shock, membrane active proteins, or non-lipid additives in the future.

Supplementary data to this article can be found online at http://dx.doi.org/10.1016/j.bbamem.2013.10.009.

Acknowledgements

The authors acknowledge Dr. Radek Macháň and Dr. Rachel S. Kraut for the very informative discussions, John A. Dangerfield for giving us the GFP–GPI construct and Shuangru Huang for the help with cell and molecular biology. N.B. is supported by a graduate scholarship of the National University of Singapore. T.W. gratefully acknowledges the funding by the Ministry of Education Singapore (MOE2012-T2-1-101).

References

[1] D. Lingwood, K. Simons, Lipid rafts as a membrane-organizing principle, Science 327 (2010) 46–50.
[2] D.M. Owen, A. Magenau, D. Williamson, K. Gaus, The lipid raft hypothesis revisited—new insights on raft composition and function from super-resolution fluorescence microscopy, Bioessays 34 (2012) 739–747.
[3] K. Simons, J.L. Sampaio, Membrane organization and lipid rafts, Cold Spring Harb. Perspect. Biol. 3 (2011) a004697.
[4] L.J. Pike, Rafts defined: a report on the Keystone symposium on lipid rafts and cell function, J. Lipid Res. 47 (2006) 1597–1598.
[5] L.J. Pike, The challenge of lipid rafts, J. Lipid Res. 50 (2009) S323–S328.
[6] G. van Meer, D.R. Voelker, G.W. Feigenson, Membrane lipids: where they are and how they behave, Nat. Rev. Mol. Cell Biol. 9 (2008) 112–124.
[7] E.L. Elson, E. Fried, J.E. Dolbow, G.M. Genin, Phase separation in biological membranes: integration of theory and experiment, Annu. Rev. Biophys. 39 (2010) 207–226.
[8] A.K. Kenworthy, N. Petranova, M. Edidin, High-resolution FRET microscopy of cholera toxin B-subunit and GPI-anchored proteins in cell plasma membranes, Mol. Biol. Cell 11 (2000) 1645–1655.
[9] K. Simons, D. Toomre, Lipid rafts and signal transduction, Nat. Rev. Mol. Cell Biol. 1 (2000) 31–41.
[10] L. Rajendran, K. Simons, Lipid rafts and membrane dynamics, J. Cell Sci. 118 (2005) 1099–1102.
[11] K.G. Suzuki, Lipid rafts generate digital-like signal transduction in cell plasma membranes, Biotechnol. J. 7 (2012) 753–761.
[12] K. Simons, M.J. Gerl, Revitalizing membrane rafts: new tools and insights, Nat. Rev. Mol. Cell Biol. 11 (2010) 688–699.
[13] M.F. Hanzal-Bayer, J.F. Hancock, Lipid rafts and membrane traffic, FEBS Lett. 581 (2007) 2098–2104.
[14] M.A. Alonso, J. Millan, The role of lipid rafts in signalling and membrane trafficking in T lymphocytes, J. Cell Sci. 114 (2001) 3957–3965.
[15] C.M. Rosenberger, J.H. Brumell, B.B. Finlay, Microbial pathogenesis: lipid rafts as pathogen portals, Curr. Biol. 10 (2000) R823–R825.
[16] F. Lafont, F.G. van der Goot, Bacterial invasion via lipid rafts, Cell. Microbiol. 7 (2005) 613–620.
[17] M. Dykstra, A. Cherukuri, H.W. Sohn, S.J. Tzeng, S.K. Pierce, Location is everything: lipid rafts and immune cell signaling, Annu. Rev. Immunol. 21 (2003) 457–481.
[18] N. Yellin, I.W. Levin, Hydrocarbon chain trans-gauche isomerization in phospholipid bilayer gel assemblies, Biochemistry 16 (1977) 642–647.
[19] C. Cametti, F. De Luca, M.A. Macri, M. Briganti, B. Maraviglia, The ripple phase in model membrane systems, Progr. Colloid. Polym. Sci. 84 (1991) 465–469.
[20] N. Kahya, P. Schwille, How phospholipid–cholesterol interactions modulate lipid lateral diffusion, as revealed by fluorescence correlation spectroscopy, J. Fluoresc. 16 (2006) 671–678.
[21] P.F. Almeida, W.L. vaz, Lateral diffusion in membranes, Handbook of Biological Physics, vol. 1, Elsevier Science B. V., 1995, pp. 305–357.
[22] P.G. Saffman, M. Delbruck, Brownian motion in biological membranes, Proc. Natl. Acad. Sci. U. S. A. 72 (1975) 3111–3113.
[23] E.P. Petrov, P. Schwille, Translational diffusion in lipid membranes beyond the Saffman–Delbruck approximation, Biophys. J. 94 (2008) L41–L43.
[24] S. Ramadurai, A. Holt, V. Krasnikov, G. van den Bogaart, J.A. Killian, B. Poolman, Lateral diffusion of membrane proteins, J. Am. Chem. Soc. 131 (2009) 12650–12656.
[25] K. Weiβ, A. Neef, Q. Van, S. Kramer, I. Gregor, J. Enderlein, Quantifying the diffusion of membrane proteins and peptides in black lipid membranes with 2-focus fluorescence correlation spectroscopy, Biophys. J. 105 (2013) 455–462.
[26] Y. Gambin, R. Lopez-Esparza, M. Reffay, E. Sierecki, N.S. Gov, M. Genest, R.S. Hodges, W. Urbach, Lateral mobility of proteins in liquid membranes revisited, Proc. Natl. Acad. Sci. U. S. A. 103 (2006) 2098–2102.
[27] G. Guigas, M. Weiss, Influence of hydrophobic mismatching on membrane protein diffusion, Biophys. J. 95 (2008) L25–L27.
[28] H.J. Galla, W. Hartmann, U. Theilen, E. Sackmann, On two-dimensional passive random walk in lipid bilayers and fluid pathways in biomembranes, J. Membr. Biol. 48 (1979) 215–236.
[29] P.B. Macedo, T.A. Litovitz, On the relative roles of free volume and activation energy in the viscosity of liquids, J. Chem. Phys. 42 (1965) 245–256.
[30] W.L. Vaz, R.M. Clegg, D. Hallmann, Translational diffusion of lipids in liquid crystalline phase phosphatidylcholine multibilayers. A comparison of experiment with theory, Biochemistry 24 (1985) 781–786.
[31] A. Filippov, G. Oradd, G. Lindblom, The effect of cholesterol on the lateral diffusion of phospholipids in oriented bilayers, Biophys. J. 84 (2003) 3079–3086.
[32] E. Falck, M. Patra, M. Karttunen, M.T. Hyvonen, I. Vattulainen, Lessons of slicing membranes: interplay of packing, free area, and lateral diffusion in phospholipid/cholesterol bilayers, Biophys. J. 87 (2004) 1076–1091.
[33] S. Chiantia, J. Ries, P. Schwille, Fluorescence correlation spectroscopy in membrane structure elucidation, Biochim. Biophys. Acta 1788 (2009) 225–233.
[34] R. Machan, M. Hof, Lipid diffusion in planar membranes investigated by fluorescence correlation spectroscopy, Biochim. Biophys. Acta 1798 (2010) 1377–1391.
[35] R. Machan, M. Hof, Recent developments in fluorescence correlation spectroscopy for diffusion measurements in planar lipid membranes, Int. J. Mol. Sci. 11 (2010) 427–457.
[36] B. Kannan, L. Guo, T. Sudhaharan, S. Ahmed, I. Maruyama, T. Wohland, Spatially resolved total internal reflection fluorescence correlation microscopy using an electron multiplying charge-coupled device camera, Anal. Chem. 79 (2007) 4463–4470.
[37] J. Sankaran, M. Manna, L. Guo, R. Kraut, T. Wohland, Diffusion, transport, and cell membrane organization investigated by imaging fluorescence cross-correlation spectroscopy, Biophys. J. 97 (2009) 2630–2639.
[38] N. Bag, J. Sankaran, A. Paul, R.S. Kraut, T. Wohland, Calibration and limits of camera-based fluorescence correlation spectroscopy: a supported lipid bilayer study, Chemphyschem 13 (2012) 2784–2794.
[39] L. Wawrezinieck, H. Rigneault, D. Marguet, P. Lenne, Fluorescence correlation spectroscopy diffusion laws to probe the submicron cell membrane organization, Biophys. J. 89 (2005) 4029–4042.
[40] A.A. Brian, H.M. McConnell, Allogeneic stimulation of cytotoxic T cells by supported planar membranes, Proc. Natl. Acad. Sci. U. S. A. 81 (1984) 6159–6163.
[41] J. Sankaran, X. Shi, L.Y. Ho, E.H. Stelzer, T. Wohland, ImFCS: a software for imaging FCS data analysis and visualization, Opt. Express 18 (2010) 25468–25481.
[42] J. Sankaran, N. Bag, R.S. Kraut, T. Wohland, Accuracy and precision in camera-based fluorescence correlation spectroscopy measurements, Anal. Chem. 85 (2013) 3948–3954.
[43] V. Ruprecht, S. Wieser, D. Marguet, G.J. Schutz, Spot variation fluorescence correlation spectroscopy allows for superresolution chronoscopy of confinement times in membranes, Biophys. J. 100 (2011) 2839–2845.
[44] M. Javanainen, L. Monticelli, J. Bernardino de la Serna, I. Vattulainen, Free volume theory applied to lateral diffusion in Langmuir monolayers: atomistic simulations for a protein-free model of lung surfactant, Langmuir 26 (2010) 15436–15444.
[45] Z. Derzko, K. Jacobson, Comparative lateral diffusion of fluorescent lipid analogues in phospholipid multibilayers, Biochemistry 19 (1980) 6050–6057.
[46] N. Kucerka, M.P. Nieh, J. Katsaras, Fluid phase lipid areas and bilayer thicknesses of commonly used phosphatidylcholines as a function of temperature, Biochim. Biophys. Acta 1808 (2011) 2761–2771.
[47] A. Arnold, M. Paris, M. Auger, Anomalous diffusion in a gel–fluid lipid environment: a combined solid-state NMR and obstructed random-walk perspective, Biophys. J. 87 (2004) 2456–2469.
[48] A.J. Garcia-Saez, S. Chiantia, P. Schwille, Effect of line tension on the lateral organization of lipid membranes, J. Biol. Chem. 282 (2007) 33537–33544.
[49] F.A. Heberle, R.S. Petruzielo, J. Pan, P. Drazba, N. Kucerka, R.F. Standaert, G.W. Feigenson, J. Katsaras, Bilayer thickness mismatch controls domain size in model membranes, J. Am. Chem. Soc. 135 (2013) 6853–6859.
[50] N. Kahya, Light on fluorescent lipids in rafts: a lesson from model membranes, Biochem. J. 430 (2010) e7–e9.
[51] G.S. Longo, M. Schick, I. Szleifer, Stability and liquid–liquid phase separation in mixed saturated lipid bilayers, Biophys. J. 96 (2009) 3977–3986.
[52] B.L. Stottrup, S.L. Veatch, S.L. Keller, Nonequilibrium behavior in supported lipid membranes containing cholesterol, Biophys. J. 86 (2004) 2942–2950.
[53] D. Hakobyan, A. Heuer, Phase separation in a lipid/cholesterol system: comparison of coarse-grained and united-atom simulations, J. Phys. Chem. B 117 (2013) 3841–3851.
[54] J. Pan, T. Mills, S. Tristram-Nagle, J. Nagle, Cholesterol perturbs lipid bilayers nonuniversally, Phys. Rev. Lett. 100 (2008) 198103.
[55] F.A. Heberle, G.W. Feigenson, Phase separation in lipid membranes, Cold Spring Harb. Perspect. Biol. 3 (2011).
[56] J. Pan, S. Tristram-Nagle, J. Nagle, Effect of cholesterol on structural and mechanical properties of membranes depends on lipid chain saturation, Phys. Rev. E. 80 (2009) 021931.
[57] R. Zidovetzki, I. Levitan, Use of cyclodextrins to manipulate plasma membrane cholesterol content: evidence, misconceptions and control strategies, Biochim. Biophys. Acta 1768 (2007) 1311–1324.
[58] S.A. Sanchez, G. Gunther, M.A. Tricerri, E. Gratton, Methyl-beta-cyclodextrins preferentially remove cholesterol from the liquid disordered phase in giant unilamellar vesicles, J. Membr. Biol. 241 (2011) 1–10.
[59] S. Mahammad, I. Parmryd, Cholesterol homeostasis in T cells. Methyl-beta-cyclodextrin treatment results in equal loss of cholesterol from Triton X-100 soluble and insoluble fractions, Biochim. Biophys. Acta 1778 (2008) 1251–1258.
[60] P. Winckler, A. Cailler, R. Deturche, P. Jeannesson, H. Morjani, R. Jaffiol, Microfluidity mapping using fluorescence correlation spectroscopy: a new way to investigate

plasma membrane microorganization of living cells, Biochim. Biophys. Acta 1818 (2012) 2477–2485.
[61] E. Yechiel, M. Edidin, Micrometer-scale domains in fibroblast plasma membranes, J. Cell. Biol. 105 (1987) 755–760.
[62] H.T. He, D. Marguet, Detecting nanodomains in living cell membrane by fluorescence correlation spectroscopy, Annu. Rev. Phys. Chem. 62 (2011) 417–436.
[63] S.M. Sterling, E.S. Allgeyer, J. Fick, I. Prudovsky, M.D. Mason, D.J. Neivandt, Phospholipid diffusion coefficients of cushioned model membranes determined via Z-scan fluorescence correlation spectroscopy, Langmuir 29 (2013) 7966–7974.
[64] C. Favard, J. Wenger, P.F. Lenne, H. Rigneault, FCS diffusion laws in two-phase lipid membranes: determination of domain mean size by experiments and Monte Carlo simulations, Biophys. J. 100 (2011) 1242–1251.
[65] E. Sezgin, I. Levental, M. Grzybek, G. Schwarzmann, V. Mueller, A. Honigmann, V.N. Belov, C. Eggeling, U. Coskun, K. Simons, P. Schwille, Partitioning, diffusion, and ligand binding of raft lipid analogs in model and cellular plasma membranes, Biochim. Biophys. Acta 1818 (2012) 1777–1784.
[66] C. Kuo, R.M. Hochstrasser, Super-resolution microscopy of lipid bilayer phases, J. Am. Chem. Soc. 133 (2011) 4664–4667.
[67] P.F. Lenne, L. Wawrezinieck, F. Conchonaud, O. Wurtz, A. Boned, X.J. Guo, H. Rigneault, H.T. He, D. Marguet, Dynamic molecular confinement in the plasma membrane by microdomains and the cytoskeleton meshwork, EMBO J. 25 (2006) 3245–3256.
[68] V.A. Frolov, Y.A. Chizmadzhev, F.S. Cohen, J. Zimmerberg, "Entropic traps" in the kinetics of phase separation in multicomponent membranes stabilize nanodomains, Biophys. J. 91 (2006) 189–205.
[69] C. Eggeling, C. Ringemann, R. Medda, G. Schwarzmann, K. Sandhoff, S. Polyakova, V.N. Belov, B. Hein, C. von Middendorff, A. Schonle, S.W. Hell, Direct observation of the nanoscale dynamics of membrane lipids in a living cell, Nature 457 (2009) 1159–1162.